The Journal of Neuroscience, December 1, 1996, *16*(23):7733–7741

Visual Response Properties of Striate Cortical Neurons Projecting to Area MT in Macaque Monkeys

J. Anthony Movshon[1] and William T. Newsome[2]

[1]*The Howard Hughes Medical Institute, and Center for Neural Science and Department of Psychology, New York University, New York, New York 10003, and* [2]*Department of Neurobiology, Stanford University School of Medicine, Stanford, California 94305*

We have previously shown that some neurons in extrastriate area MT are capable of signaling the global motion of complex patterns; neurons randomly sampled from V1, on the other hand, respond only to the motion of individual oriented components. Because only a small fraction of V1 neurons projects to MT, we wished to establish the processing hierarchy more precisely by studying the properties of those neurons projecting to MT, identified by antidromic responses to electrical stimulation of MT. The neurons that project from V1 to MT were directionally selective and, like other V1 neurons, responded only to the motion of the components of complex patterns. The projection neurons were predominantly "special complex," responsive to a broad range of spatial and temporal frequencies, and sensitive to very low stimulus contrasts. The projection neurons thus comprise a homogeneous and highly specialized subset of V1 neurons, consistent with the notion that V1 acts as clearing house of basic visual measurements, distributing information appropriately to higher cortical areas for specialized analysis.

Key words: visual cortex; motion processing; visual receptive fields; cortico-cortical projections; antidromic activation; direction selectivity

Psychophysical evidence suggests that motion processing within the central visual system occurs in at least two stages. In the first stage, orientation- and spatial frequency-selective mechanisms compute motion signals within local regions of visual space. The local motion signals encoded at this stage, considered individually, are inherently ambiguous because an orientation-selective mechanism can only signal motion in a direction orthogonal to its preferred axis of orientation. The ambiguous first stage signals, however, can be combined according to simple geometric rules to yield a second stage of motion processing in which the direction and speed of complex moving objects are represented veridically (Adelson and Movshon, 1982; Movshon et al., 1985; Ferrera and Wilson, 1990; Wilson et al., 1992).

Physiological investigation of the visual cortex of monkeys has revealed potential correlates of these two processing stages in striate cortex (V1) and extrastriate area MT (V5), respectively (Movshon et al., 1985; Rodman and Albright, 1989). In these studies, directionally selective neurons were driven with superimposed, drifting sine wave gratings as visual stimuli. Under appropriate conditions, human observers viewing such stimuli see a coherently moving "plaid" pattern whose perceived direction of motion differs from that of either component grating (Adelson and Movshon, 1982). Orientation-selective neurons in V1 responded overwhelmingly to the motion of the individual component gratings, not to the overall motion of the plaid pattern perceived by human observers. In MT, however, roughly one third of the neurons encoded the direction of the plaid pattern.

These findings naturally suggest that direction-selective neurons in V1 and MT are the neural correlates of the hypothesized first and second stages of motion processing (for a recent review, see Stoner and Albright, 1994). This issue remains unresolved, however, because presently available data cannot rule out the possibility that the minority of V1 neurons *that actually projects to MT* might differ in important ways from the neurons examined in random samples from V1. The key questions are (1) whether the projection neurons are directionally selective at all, and (2) whether the projection neurons respond to plaid patterns in a manner characteristic of the first ("component") or second ("pattern") stage of motion processing.

To resolve this issue, we studied a population of V1 neurons that were antidromically activated by electrical stimulation of MT. The large majority of these neurons were strongly directional and responded selectively to the motion of the component gratings of plaid patterns. The MT projection neurons were typically "special complex" cells responding to a broad range of spatial and temporal frequencies. Our observations support the notion that V1 and MT are, respectively, important neural substrates for the first and second stages of motion processing.

These results have been briefly reported elsewhere (Movshon and Newsome, 1984).

MATERIALS AND METHODS

Preparation and maintenance. Experiments (3–4 d in duration) were performed on four young adult monkeys (*Macaca fascicularis*) weighing between 3.2 and 3.4 kg. After induction of anesthesia with ketamine, a saphenous vein was cannulated and intravenous anesthesia (Pentathol) was used for the duration of surgery. The trachea was cannulated, and the animal's head was positioned in a stereotaxic frame. A craniotomy was made over occipital cortex that permitted microelectrode access both to V1 and MT. Openings were made in the dura, and the exposed region was covered with warm agar.

Received May 10, 1996; revised Sept. 3, 1996; accepted Sept. 9, 1996.

This work was supported by grants from the National Eye Institute (EY 02017) and the National Science Foundation (BNS 82-16950). During these experiments, W.T.N. was at the Laboratory of Sensorimotor Research, National Eye Institute, National Institutes of Health (Bethesda, MD).

Correspondence should be addressed to J. Anthony Movshon, Center for Neural Science, New York University, 4 Washington Place, Room 809, New York, NY 10003-6621.

After surgery was complete, paralysis was induced and maintained with an infusion of pancuronium bromide (Pavulon, 0.1 mg/kg/hr) in Ringer solution with dextrose (5–10 ml/hr). Animals were artificially respired with a mixture of N_2O, O_2, and CO_2 (typically 58:40:2). Either the respirator stroke volume or the CO_2 concentration in the gas mixture could be adjusted to maintain peak expired CO_2 near 4.0%. A thermostatically controlled heating pad helped maintain rectal temperature near 37°C. Anesthesia was maintained by artificial respiration with the gas mixture described above supplemented with intravenous infusion of sodium pentobarbital (1–4 mg/kg/hr). Both the EEG and the EKG were monitored throughout the experiment to assess the adequacy of anesthesia and the general physiological condition of the animal.

Topically applied atropine was used to dilate the pupils and stabilize accommodation. Zero-power contact lenses protected the corneas, and supplementary lenses were used to make the retinas conjugate with a tangent screen and CRT display that were 57 cm distant. The contact lenses were removed and cleaned periodically, and the eyes were rinsed with saline. In addition, the lenses were removed for a period of a few hours each day, during which an ophthalmic antibiotic solution was administered and the eyelids closed. A reversible ophthalmoscope was used to plot the positions of the foveas at regular intervals throughout the experiment.

Recording and electrical stimulation. In each experiment, MT was first located by microelectrode recordings. We then inserted a low-impedance stimulating electrode into a region of MT representing the inferior contralateral quadrant of the visual field, ~5 deg from the center of gaze. We plotted the composite visual receptive field of neurons near the tip of the stimulating electrode by attending to the weak "swish" response evoked by hand-held search stimuli. The recording location in V1 was then chosen, based on standard maps (e.g., Van Essen et al., 1984), so that V1 receptive fields were superimposed on some portion of the MT receptive field as assessed through the stimulating electrode.

We stimulated MT by delivering single 50 μsec electrical pulses through a bipolar stimulating electrode; the uninsulated tips were ~0.5 mm in length and separated by 1 mm (Rhodes Medical, 30–35 kΩ). The stimulating pulses were bipolar. Current thresholds for antidromically activated neurons were typically 0.5–2.5 mA, although we frequently tested higher currents (up to 30 mA) so as to detect any higher-threshold axons; thresholds for orthodromic activation were often higher, up to 10–20 mA. Delivery of the stimulation pulse was confirmed by a brief electrical artifact recorded by the V1 electrode. Oscilloscope sweeps were triggered on the electrical stimulus pulse and superimposed to detect activation of V1 neurons by stimulation of MT. We used only a single, bipolar stimulating electrode to confine current spread as closely as possible to the gray matter of MT. Portions of the optic radiation course beneath the floor of the superior temporal sulcus near MT, and we wished to minimize the possibility of antidromically activating cortico-thalamic fibers originating in V1.

Neuronal signals from V1, recorded with tungsten-in-glass microelectrodes (Merrill and Ainsworth, 1972), were conventionally amplified and displayed. Action potentials of single units were isolated while the cortex was activated with simple visual search stimuli. For quantitative analyses, each action potential triggered a standard pulse from a window discriminator, which was sent to a computer for storage and analysis.

For each neuron that was reliably activated with minimal latency jitter by stimulation of MT, we conducted a collision test for antidromic activation (Bishop et al., 1962). Figure 1 illustrates the results of such a test for one V1 neuron. The superimposed traces in Figure 1*A* show that the neuron reliably generated a single spike (indicated by the *arrow*) 1.4 msec after the electrical stimulus artifact (indicated by the *asterisk*). In Figure 1*B*, we triggered the electrical stimulation of MT from a spontaneous action potential from the V1 neuron (indicated by the *circle*). We systematically varied the delay between the spontaneous action potential and delivery of the electrical stimulus to MT. For the longest delay tested (2.4 msec, *top right*), the electrical stimulus in MT elicited a short latency action potential from the V1 neuron on every trial. For an intermediate delay (2.0 msec, *middle right*), electrical stimulation occasionally failed to generate an action potential from the V1 neuron. For the shortest delay (1.8 msec, *bottom right*), electrical stimulation failed to elicit an action potential in V1, demonstrating collision of the spontaneous orthodromic spike with the electrically elicited antidromic spike. We considered a V1 neuron to be antidromically activated from MT only if it passed a collision test in this manner.

Visual stimulation. We initially mapped the receptive fields of each neuron on a tangent screen, using rear-projected geometric targets such as spots, slits, and edges. Colored filters could be interposed in the projector beam for rudimentary tests of color selectivity. The visual stimuli used for quantitative experiments were moving sinusoidal gratings or plaid patterns generated by a PDP 11/34 computer on the face of a Tektronix 608 oscilloscope (P31 phosphor). The display subtended ~6 deg at the animal's eyes, and the mean luminance was held constant at 40 cd/m^2. The frame rate of the display was 128 Hz. The receptive field of each cell encountered was classified as simple, complex, end-stopped, or nonoriented according to the criteria of Hubel and Wiesel (1968), supplemented by information on the form of responses to sinusoidal gratings (Movshon et al., 1978; DeValois et al., 1982; Skottun et al., 1991). For each neuron, we assessed the eye dominance and optimal orientation and direction of motion, if any. If the neuron was activated antidromically from MT, we estimated the most effective spatial and temporal frequencies using sinusoidal gratings of the optimal orientation and direction of motion. If the quality of the recorded signal permitted it, we then studied the neuron quantitatively. All receptive field measurements were made through the eye that more effectively activated the neuron.

Our main goal was to compare the selectivity of the neurons for the direction of motion of plaid and grating patterns, and for this we used methods that we have detailed elsewhere (Gizzi et al., 1990) (see also Movshon et al., 1985). The stimuli were presented within an aperture that was usually 6 deg in diameter, but was electronically windowed to smaller dimensions if the cell's response was significantly better for smaller targets. Plaid stimuli were generated by interleaving frames displaying two drifting sinusoidal gratings whose orientations differed by 90 or 135 deg. The spatial frequency and contrast were the same for the two "component" gratings and were set to the optimal values for single grating stimuli. Direction tuning curves were obtained for both grating and plaid patterns. The direction of motion was varied around the clock in 22.5 deg increments, and the grating and plaid patterns of various motion directions were presented in a single, pseudorandomly ordered

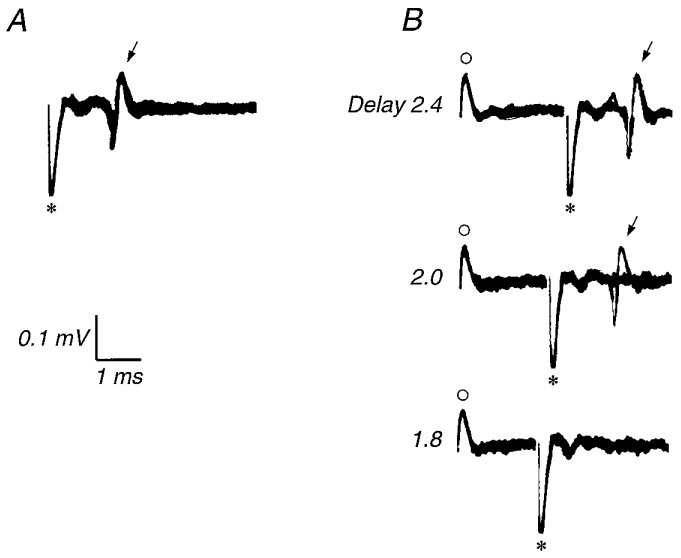

Figure 1. Collision test for identifying antidromically activated neurons. *A*, Ten superimposed traces; each shows an electrical stimulus artifact (*), followed 1.4 msec later by an action potential (*arrow*). Note the absence of discernible latency jitter in the response. *B*, Electrical activation of MT was triggered on a spontaneous action potential generated by the V1 neuron. The temporal interval between the spontaneous action potential and electrical stimulus was systematically varied from 2.4 to 1.8 msec. The first deflection in each trace (*circle*) is the spontaneous action potential, the second (*) is the electrical stimulus artifact, and third (*top two traces* only, *arrow*) is the antidromic action potential. Each trace shows the superimposition of five trials. When the interval between the spontaneous action potential and the electrical stimulus was 2.4 msec (*top*), the electrical stimulus elicited an antidromic action potential that never failed to reach the recording electrode in V1. When the interval was 1.8 msec (*bottom*), the antidromic action potential never reached V1 because it collided with the spontaneous orthodromic action potential. For an intermediate interval of 2.0 msec, the antidromic action potential reached V1 only once, being blocked by collision on the other four trials.

sequence of trials. If time permitted, we also made quantitative measurements of the spatial and temporal frequency tuning for each neuron and of other receptive field properties of interest.

Histology and track reconstructions. During recording, electrolytic marking lesions were made at points of interest along each track by passing DC current (1–2 μA for 2–5 sec, tip-negative) through the electrode tip. At the end of the experiment, the animals were killed with an overdose of Nembutal and perfused through the heart with 0.1 M PBS followed by a 4% solution of paraformaldehyde in PBS. Tissue blocks containing the region of interest were equilibrated in 30% sucrose, then cut in 40 μm sections on a freezing microtome. Sections at regular intervals through V1 and MT were stained for cell bodies with cresyl violet.

In two monkeys, a series of sections was also stained for myelinated fibers by the method of Gallyas (1979) to confirm placement of the stimulating electrode within the heavily myelinated borders of MT (Allman and Kaas, 1971; Ungerleider and Mishkin, 1979; Van Essen et al., 1981). In the other two animals, the location of the stimulating electrode was confirmed by its general location on the posterior bank of the superior temporal sulcus and by the direction-selective responses obtained through microelectrode recordings in the same location.

Electrode tracks in V1 were reconstructed using information from several sources: (1) marking lesions made during the experiment, (2) recorded depths of entrances to and exits from gray matter, and (3) recorded depths of physiologically recognizable landmarks such as the high concentration of nonoriented cells and elevated spontaneous discharge of layer 4c, or the characteristic direction selectivity of layer 4b (Dow, 1974; Blasdel and Fitzpatrick, 1984; Livingstone and Hubel, 1984; Hawken et al., 1988). In general, these corroborated each other well.

RESULTS

Prevalence and latency of electrical activation

Figure 2 is diagram of a single vertical penetration through V1. The brain was sectioned parasagittally. The electrode track crossed V1 at three different locations—on the dorsal operculum, in the head of the calcarine sulcus, and in the external calcarine sulcus in the ventral operculum. The inset at the lower right of Figure 2 shows a map of the central visual field on which are marked the centers of the receptive fields encountered at each of the three recording locations in V1 (*points*) and the multiunit receptive field recorded through the low impedance-stimulating electrode in MT (*stippled rectangle*). All three V1 receptive fields lay within the boundaries of the MT receptive field.

We recorded from 67 isolated V1 neurons in this penetration. Each horizontal tick mark indicates the location of a recorded cell that was not activated by electrical stimulation of MT. Solid circles represent neurons that were orthodromically activated from MT, and the star shows the location of the single antidromically activated neuron encountered in this penetration.

This penetration illustrates several features that were typical of our data set as a whole. (1) Orthodromically driven cells were encountered much more commonly than antidromically activated cells and were scattered throughout the cortical layers. In all we studied 745 neurons in 15 microelectrode penetrations that traversed in aggregate 102.5 mm of cortex. Of these 745, we identified 94 orthodromically driven cells (12.6%) but only 12 antidromically driven cells (1.6%). (2) Antidromically driven cells, when found, conformed well to the known laminar pattern of projections from V1 to MT. This projection arises exclusively from layers 4b and the solitary cells of Meynert near the boundary of layers 5 and 6, with layer 4b neurons outnumbering layer 5–6 neurons by ~20:1 (Lund et al., 1976; Spatz, 1977; Tigges et al., 1981; Maunsell and Van Essen, 1983; Weller et al., 1984; Ungerleider and Desimone, 1986; Shipp and Zeki, 1989). The single antidromically activated cell found in the penetration shown in Figure 2 fell into the latter category. Of the 12 antidromically activated neurons we encountered, 6 were located in layer 4b and 6 were found near the boundary of layers 5 and 6. (3) We failed

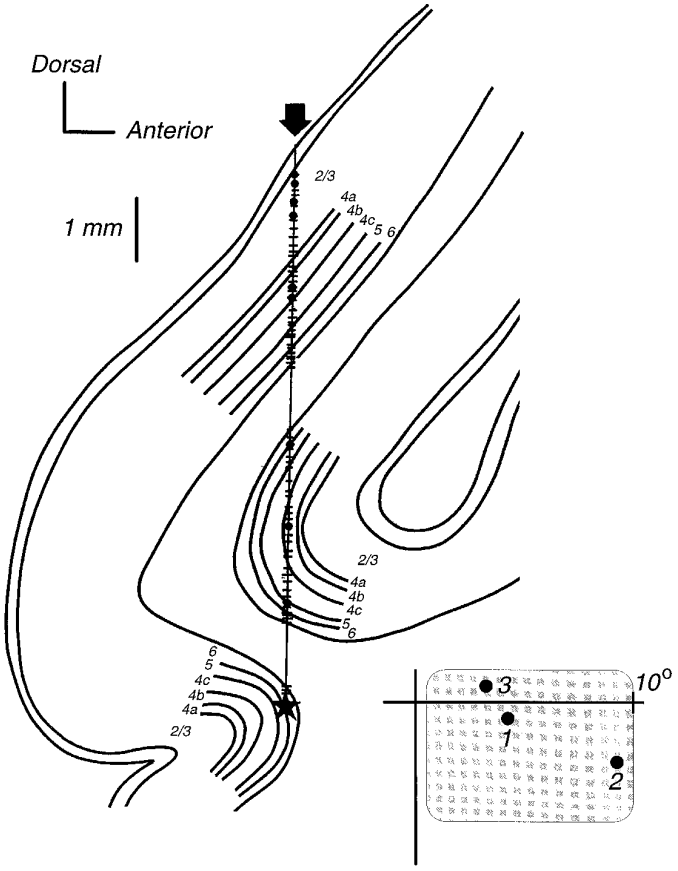

Figure 2. Example penetration through V1 (parasagittal section). *Solid circles* indicate neurons that were orthodromically activated from MT; the *star* represents the single neuron that was antidromically activated. *Tick marks* show neurons that were isolated and tested, but were not driven from MT. The *inset* shows the receptive field location at the MT recording site (*stippled*) as well as the receptive field centers in the three segments V1 of V1 gray matter: dorsal operculum (*1*), calcarine sulcus (*2*), and ventral operculum (*3*).

to detect antidromically activated cells in many locations where conditions appeared to be ideal for finding such neurons. In the illustrated penetration, for example, we recorded from 12 neurons in or near layer 4b, with receptive fields contained within the MT multiunit receptive field at the end of the stimulating electrode. Frequently these neurons were strongly directional, yet none was antidromically activated. This was rather trying. It was our impression that alignment of the visual receptive fields of the V1 neurons with the MT multiunit field was critical—most of our antidromically activated neurons had receptive fields near the center or "hot spot" of the MT multiunit field, and our success rate was discernibly lower when the V1 receptive fields were near the edge of the MT multiunit field. Receptive field alignment seemed less critical for obtaining orthodromic activation.

Figure 3 shows the distribution of latencies for the 106 V1 neurons that were electrically driven by stimulation of MT. The filled bars indicate the antidromically activated neurons. The open bars illustrate the latencies of orthodromically activated neurons. The firing of these neurons was often less reliable and more variable in timing than antidromic activation, as would be expected from synaptically mediated activation. We estimated latency from the time of the first reliable spike from at least 10 superimposed oscilloscope traces. Not surprisingly, antidromic

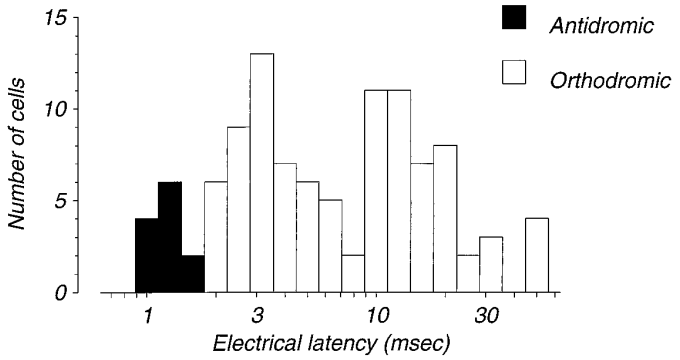

Figure 3. Frequency histogram of activation latencies for all neurons driven by electrical stimulation in MT. *Dark bars* represent antidromically activated neurons; *open bars* indicate orthodromically activated neurons.

neurons yielded the shortest latencies (range 1.0–1.7 msec), with values tightly clustered around a mean of 1.3 msec. The mean latency for layer 4b neurons was 1.4 msec, and for layer 5/6 neurons was 1.2 msec but, given the small number of cells, it is not surprising that this difference was not statistically significant.

The distribution of orthodromic latencies ranged between 2.0 and 50 msec, with two broad modes, one near 3 msec and a second near 12 msec. The interpretation of the orthodromically elicited firing patterns is not straightforward. It is tempting to suppose that they reflect the feedback action exerted by projections from MT on V1 cells. However, we encountered substantial numbers of orthodromically activated neurons in layers (such as layer 2) that do not receive feedback projections from MT (see Fig. 2). What is known about the anatomical patterns of projection in V1 suggests that the activation of these neurons was due to recurrent collaterals of neurons antidromically driven from MT (Blasdel et al., 1985); it is conceivable that this is the principal route by which some of our "orthodromically activated" neurons received their signals from MT. Many neurons with latencies between 2 and 6 msec (the first mode of the distribution in Fig. 3) were found in layers known to receive feedback projections; these are more likely to be activated by fairly direct feedback pathways from MT to V1. The considerably longer latencies of neurons in the second mode likely reflect more indirect activation paths, possibly involving a cascade of connections between MT and V1, and certainly defy simple interpretation.

Receptive field properties of electrically activated neurons

The 94 neurons orthodromically activated from MT were heterogeneous in their properties, including cells with both simple and complex receptive fields, cells with and without directional selectivity or color selectivity, and cells with all degrees of binocular interaction. Although we did not make a quantitative study of their properties, our qualitative data suggest that these neurons represented a more or less uniform cross section of the V1 neuronal population. The only important physiological cell type that was apparently not represented was the monocularly driven, nonoriented, concentrically organized type characteristically found in layer 4c. As noted above, it is not clear whether this heterogeneity reflects a nonspecific feedback from MT to V1, or more complex properties of intracortical circuits.

In contrast, the antidromically driven neurons formed a distinctive and homogeneous group in terms of their visual receptive field properties. As mapped using hand-held targets, all 12 neurons had orientation-selective visual receptive fields of the complex type. In most cases, moreover, these neurons appeared to be "special complex," because they responded optimally to a bar much shorter than the length of the receptive field (Palmer and Rosenquist, 1974; Gilbert, 1977). All were binocularly activated, and 11 of the 12 (92%) were in eye dominance groups 3–5; only 204 of 465 (44%) of the neurons that were not antidromically activated and whose binocularity was assessed fell into these groups. All antidromic neurons were either directionally selective or directionally biased. Because the preferred directions of some layer 4b neurons have been reported to reverse with stimulus contrast (Livingstone and Hubel, 1984), we routinely assessed direction selectivity with both light and dark bars. In all cases tested, the preferred direction was independent of the contrast of the stimulus. None showed prominent selectivity for the color of the stimulus. Finally, antidromically activated neurons tended to be unusually sensitive to low stimulus contrasts, and broadly tuned for the spatial and temporal frequency of grating targets. A detailed analysis of the properties of these neurons is the subject of the remainder of the paper.

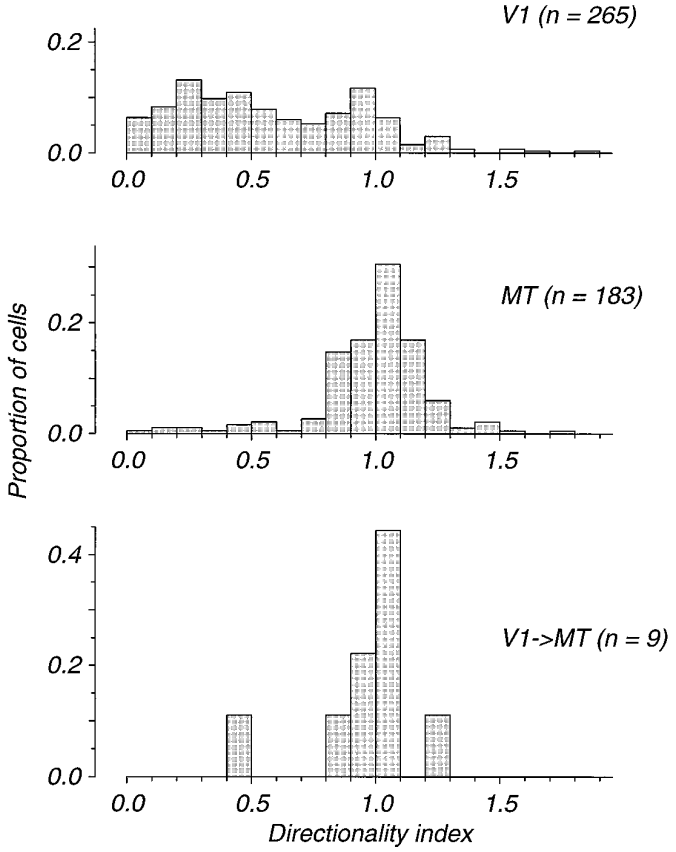

Figure 4. Frequency histograms of directionality indices for randomly sampled V1 neurons (*top*), randomly sampled MT neurons (*middle*), and V1 neurons antidromically activated from MT (*bottom*). The directionality index is described in the text.

Directional selectivity of antidromically activated neurons

Of the 12 neurons antidromically activated from MT, we collected quantitative data on 9. The remaining 3 were lost soon after qualitative characterization or were insufficiently well isolated for quantitative analysis. Figure 4 compares the direction selectivity of antidromically activated neurons with random samples of V1

and MT neurons recorded in the same laboratory. To characterize directional selectivity, we used the familiar direction index (DI) given by the expression $1 - n/p$, where p is the neuron's response to motion in the optimal (preferred) direction and n is the response to motion in the direction 180 deg opposite to the optimal (null direction). We considered the neuron's "response" to be the average number of spikes occurring during presentation of the visual stimulus, less the spontaneous firing rate. This index assumes values near zero for nondirectional cells and values near unity for highly directional cells. The index may exceed 1 if the neuron's activity is inhibited below the spontaneous level by null direction motion (i.e., a "negative" response).

Interestingly, the subset of V1 neurons projecting to MT conformed much more closely to the directional properties of MT neurons than of V1 neurons considered as a whole. Most projection neurons were highly directional (mean DI = 0.96), and the distribution of direction indices for these neurons was indistinguishable from that for MT neurons (mean DI = 0.99). In addition, the three antidromically activated neurons that were not characterized quantitatively were all direction-selective by qualitative assessment. Clearly, a physiologically specialized subset of V1 neurons projects to MT, raising the possibility that MT inherits many of its motion encoding properties directly from V1. It is therefore critical to know whether the V1 neurons that project to MT neurons themselves express the pattern direction-selective response properties of MT neurons.

Figure 5 shows tests of pattern direction selectivity performed for two antidromically activated V1 neurons (Movshon et al., 1985; Gizzi et al., 1990). Figure 5, *A* and *C*, shows directional tuning curves obtained using a single sinusoidal grating drifted in 16 different directions through the receptive field. Each neuron neuron responded best to nearly rightward motion and had a tuning bandwidth of ~60°.

The solid curves and symbols in Figure 5, *B* and *D*, show the directional tuning of each neuron to a plaid stimulus composed of two sinusoidal gratings separated in orientation by 135°. The labeled directions on the polar plot correspond to the direction of motion of the plaid stimulus. For a plaid moving directly rightward, therefore, one of the component gratings moved up and to the right while the second component grating moved down and to the right. If the neuron responded to the direction of motion of the stimulus (i.e., it was pattern direction-selective), the directional tuning curve for the plaid stimulus should have been essentially the same as the tuning curve for the single grating in Figure 5, *A* and *C*, with a single, well defined peak for nearly rightward motion. If, on the other hand, the neuron responded individually to the oriented component gratings (i.e., it was component direction-selective), the tuning curves for the plaid stimulus should have conformed to the predicted tuning curves (*dotted line*) in Figure 5, *B* and *D*, which are calculated simply from the sum of the two tuning curves expected if the cells responded independently to each of the component gratings. The predicted curve is bilobed in each case because one or the other component grating moves in the neuron's preferred direction (rightward) when the global motion of the plaid is either obliquely up and right or obliquely down and right. Clearly, the plaid tuning curves for both V1 cells were bilobed, and corresponded better to the curves expected for component direction selectivity than that for pattern direction selectivity. The cell whose responses are illustrated in Figure 5, *A* and *B*, was clearly classified as component direction-selective. The cell whose responses are illustrated in Figure 5, *C* and *D*, was in fact not classifiable by our standard test (see below)

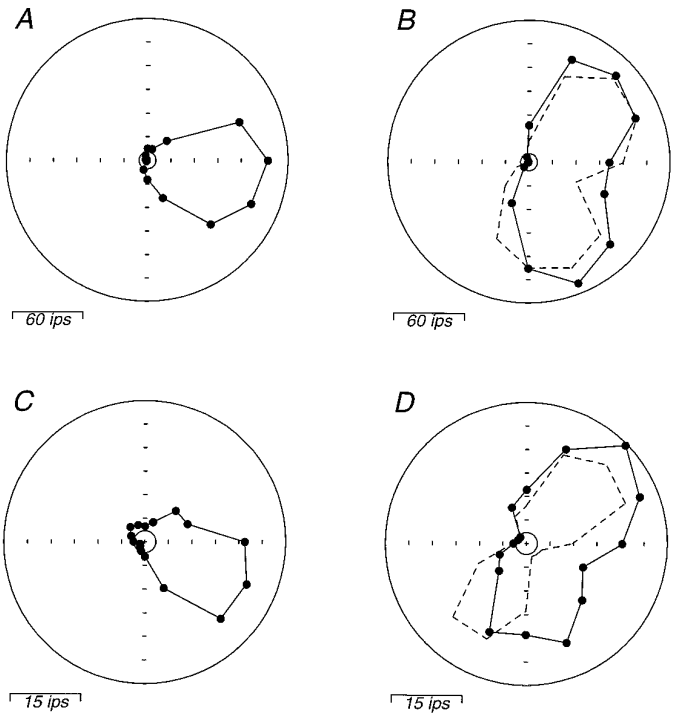

Figure 5. Direction tuning of two component direction-selective MT projection neurons to drifting sine wave gratings (*A*, *C*) and drifting plaids (*B*, *D*). Each polar plot shows the responses of the neuron to 16 directions of motion separated by equal intervals of 22.5°. The plaid stimuli were created by superimposing two sine wave gratings of equal contrast and spatial and temporal frequency, whose orientations differed by 135°. The direction of plaid motion is the direction of coherent motion perceived by human observers, which for these particular patterns lay equidistant between the directions of motion of the two component gratings. The *solid lines* and data in *B* and *D* illustrate the actual responses of the neuron; the *dashed lines* depict the predicted tuning curve if the neuron responded only to the motions of the two component gratings. The *small circles* at the center of each plot show the spontaneous firing rates.

and was the most pattern-direction-selective-like of the 9 cells we studied in this way.

We used a partial correlation analysis to quantify the degree of correspondence between the experimentally measured plaid tuning curve and the predicted tuning curves for pattern and component direction selectivity (Movshon et al., 1985; Gizzi et al., 1990). Figure 6*A* shows a scatterplot of the partial correlation coefficients calculated for each antidromically activated neuron. The abscissa shows the partial correlation between the data and the "component" prediction, whereas the ordinate shows the partial correlation between the data and the "pattern" prediction. The bullet-shaped contour divides this space into three regions of interest. Down and to the right is a region in which the correlation with the component prediction significantly exceeded the correlation with the pattern prediction or 0, whichever was larger. Neurons falling into this region most closely reflected the motion of the component gratings, and we consider such neurons to be component direction-selective. The converse relationship holds in the region up and to the left, and we consider neurons falling in this area to be pattern direction-selective. In between is a region in which cells cannot be classified as selective for either pattern or component motion. For cells in this region, neither correlation coefficient differed significantly from 0, or the two coefficients did not differ significantly from each other. For comparison, Figure 6,

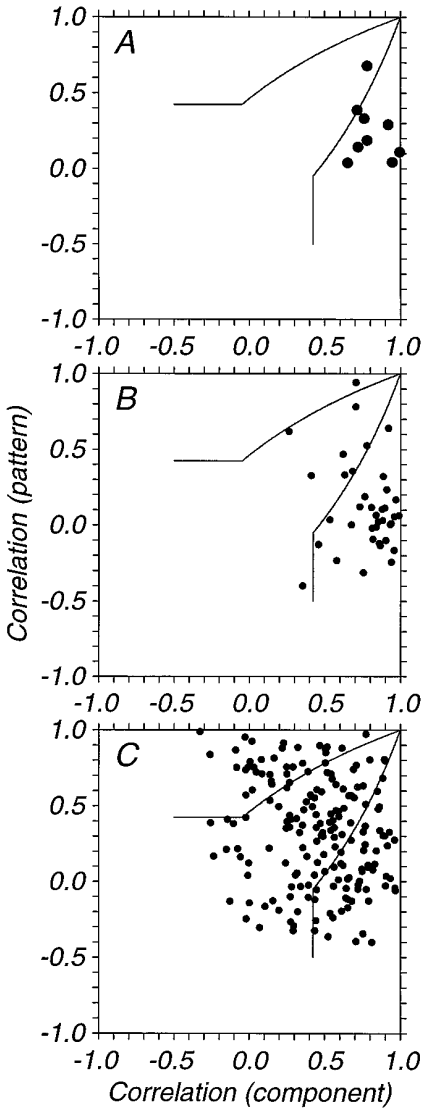

Figure 6. Partial correlation of plaid tuning curves with the predictions for component (*abscissa*) and pattern (*ordinate*) direction selectivity. The observed tuning curves were correlated with predictions derived either from the hypothesis that the plaid tuning curve was simply the sum of the independent responses of the neuron to the two components of the plaid ("component" prediction, *dashed lines* in *B*, *D*) or from the hypothesis that the plaid tuning curve was the same as the tuning curve for a single grating ("pattern" prediction, *solid lines* in *A*, *C*). To remove the influence of correlations between the predictions themselves, we calculated partial correlations R_p and R_c (for the pattern and component predictions) using the standard formulas:

$$R_p = \frac{(r_p - r_c r_{pc})}{\sqrt{(1 - r_p^2)\,(1 - r_c^2)}}$$

and

$$R_c = \frac{(r_c - r_p r_{pc})}{\sqrt{(1 - r_p^2)\,(1 - r_c^2)}},$$

where r_c and r_p are the simple correlations between the data and the component and pattern predictions, respectively, and r_{pc} is the simple correlation between the predictions. Note that these formulas were given incorrectly in earlier reports (Movshon et al., 1985; Gizzi et al., 1990). *A*, Scatterplot of the partial correlations for nine antidromically activated V1 neurons. *B*, Scatterplot for 38 randomly sampled V1 neurons. *C*, Scatterplot for 182 randomly sampled MT neurons. The different regions of each plot separated by the *curved lines* are described in the text.

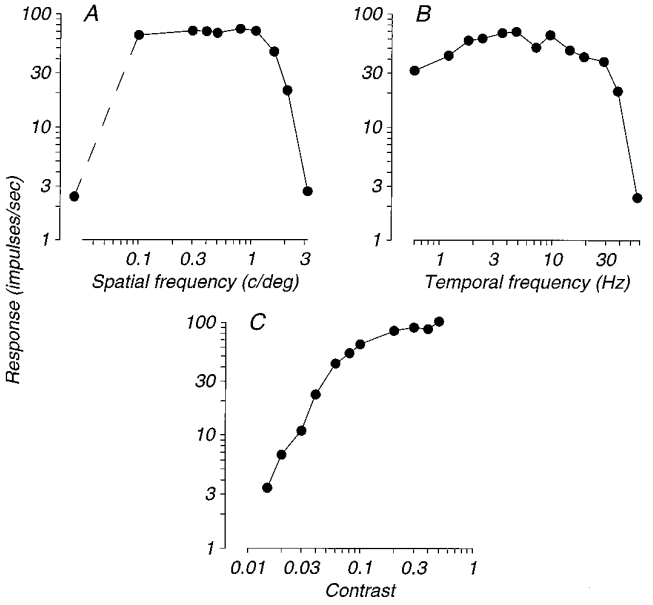

Figure 7. Responses of an antidromically driven neuron from layer 6 to sinusoidal gratings. All stimuli drifted in the preferred direction. *A*, Spatial tuning curve, measured at a drift rate of 4.8 Hz. *B*, Temporal tuning curve, measured with a spatial frequency of 0.9 c/deg. *C*, Contrast–response function, measured with gratings of 0.9 c/deg drifting at 4.8 Hz. All responses are mean firing rates with baseline firing rate subtracted.

B and *C*, shows similar scatterplots for populations of neurons randomly sampled from V1 and MT, respectively.

Of the 9 antidromically activated neurons tested quantitatively, 7 were unambiguously component direction-selective. Two neurons fell within the "unclassified" portion of the space (the upper of these points corresponds to the neuron whose tuning curves were shown in Fig. 5*C*, *D*) but were much closer to the component than to the pattern prediction. None of the 9 neurons was pattern direction-selective. Overall, the distribution from the antidromically activated neurons appeared to be indistinguishable from that observed for V1 neurons (Fig. 6*B*) and was obviously different from the much broader distribution observed for MT neurons (Fig. 6*C*).

Spatial and temporal receptive field properties of MT projection neurons

To illustrate the other receptive field properties that were typical of MT projection neurons, we show data from one such neuron (which happens to be the layer 6 neuron whose location is shown in Fig. 2).

Figure 7 shows the effect of contrast, and temporal and spatial frequency, on the responses of this neuron. The spatial frequency tuning (Fig. 7*A*) was quite broad; the neuron responded well to spatial frequencies from 0.1 to 2 c/deg. The temporal frequency tuning (Fig. 7*B*) was particularly striking: the cell responded vigorously over a broad range of frequencies extending from 0.5 to nearly 50 Hz. Figure 7*C* shows that the neuron also responded well to very low contrasts (near 0.01), and its response saturated at contrasts above 0.1. This combination of excellent temporal resolution, poor spatial resolution, and high contrast sensitivity is reminiscent of the behavior of magnocellular geniculate neurons (Derrington and Lennie, 1984) and is consistent with the predominantly magnocellular origin of visual inputs to MT (Maunsell et al., 1990).

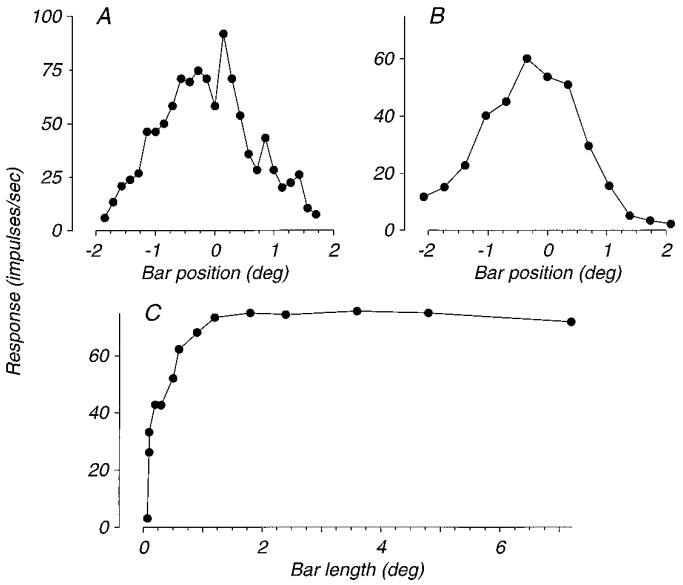

Figure 8. Responses to flashed and moving bars of the same antidromically activated neuron whose spatio-temporal properties were illustrated in Figure 7. *A*, Receptive field width profile. Neuronal response (firing rate in 80 msec of discharge containing the highest firing rate) to thin bars (0.13 deg) whose contrast was square-wave-modulated in time at 1 Hz. The neuron responded everywhere to both the dark–light and the light–dark transitions in this stimulus; the responses to light–dark transitions were consistently larger and are plotted here. *B*, Receptive field length measurement. Neuronal response (firing rate in the 80 msec of discharge containing the highest firing rate) is plotted for 13 positions of a bar 0.4° in length. This was the shortest bar that elicited a robust response as demonstrated by the length summation curve in *C*. The bar was drifted in the neuron's preferred direction at each location. The receptive field was ~3° wide. *C*, Length summation curve. Neuronal response (measured as for *B*) is plotted as a function of the length of an optimally oriented bar centered on the receptive field and drifted in the preferred direction. The response saturated for lengths greater than 1 deg, substantially less than the full 3 deg extent of the receptive field.

Figure 8 shows measurements of the spatial structure of this neuron's receptive field. Figure 8*A* shows the line-weighting function for the neuron, that is, the neuron's response to briefly flashed thin bars (0.13 deg) as a function of their position across the width of the receptive field. The receptive field was ~3 deg wide. Because the "corner" spatial frequency (Fig. 7*A*) was near 1 c/deg, 3–4 periods of the grating were contained within the receptive field, a relatively large number. Figure 8*B* shows measurements of the length profile of the neuron's receptive field. A short bright bar (0.4 deg) traversed the receptive field at 13 positions. The responses reveal that the field was ~3 deg long. Figure 8*C* shows the neuron's length summation. Bright bars of various lengths, centered on the most sensitive part of the receptive field, were swept through the receptive field. The response function rose steeply for very short bar lengths, saturating for all lengths over 1 degree. Thus in a manner characteristic of "special complex" cells (Palmer and Rosenquist, 1974; Gilbert, 1977), length summation saturated for bar lengths substantially shorter than the full width of the receptive field. This receptive field was unusually large for its eccentricity (3 × 3.5 deg); this was typically the case for antidromically activated cells located at the boundary of layers 5 and 6.

We were able to assess the spatial and temporal properties of only a subset of the MT projection neurons. The 7 neurons for which we measured spatial frequency tuning, like the example in Figure 7*A*, all had relatively broad bandwidths (1.7–3.3 octaves, compared with a geometric mean near 1.4 octaves for unselected samples of V1 neurons, e.g., DeValois et al., 1982). The 5 neurons for which we measured temporal frequency tuning, like the example in Figure 7*B*, were also relatively broadly tuned and had relatively high temporal resolution (24–55 Hz). Of the 6 neurons for which we measured contrast responses, 4 had high sensitivity and responded well to contrasts as low as 0.01–0.03, like the example in Figure 7*C*. These measurements suggest that the MT projection neurons were quite different in their spatio-temporal properties from unselected populations of V1 neurons; it is less clear, however, that they differ in their spatial and temporal properties from other directionally selective neurons in V1, which have been shown recently to have properties that are in some ways similar to those that we found for the MT projection neurons (Hawken et al., 1996).

Other than the fact that most neurons recorded near the top of layer 6 had unusually large receptive fields, we noticed no differences between these and neurons recorded in layer 4b.

DISCUSSION

The main findings of this study are that V1 neurons that project to MT are directionally selective, and that their direction selectivity is of the "component" variety. Thus the projection neurons encode the motion of the oriented components comprising a complex pattern rather than the global motion of the pattern itself. The most serious reservation about the validity of this conclusion arises from our small sample size. Only 12 of the 745 neurons tested were antidromically activated from MT, and we collected the requisite quantitative data on only 9. These 9 cells were remarkably uniform in their physiological characteristics, however, being almost exclusively component direction-selective (Figs. 4, 6). Although we cannot exclude the possibility that a few MT projection neurons are pattern direction-selective, it seems reasonable to conclude that the bulk are component direction-selective.

These results establish for the first time that MT inherits considerable directional information from V1. Directional information is not computed *de novo* in MT; rather, MT performs more complex computations based on the extensive base of local motion measurements provided by V1. This is a logical scheme for a hierarchical motion processing system, and its existence has been suspected for a number of years based on convergent data concerning the laminar organization of projection neurons from V1 to MT (e.g., Shipp and Zeki, 1989) and the laminar localization of direction-selective neurons in V1 (e.g., Hawken et al., 1988). Motion analysis in MT is not, however, totally dependent on input from V1. Directionally selective visual responses can be elicited from MT neurons after surgical lesions or reversible cooling of V1, although overall responsiveness is reduced considerably and directional tuning is cruder (Rodman et al., 1989; Girard et al., 1992). The residual directional responses in MT appear to originate from the colliculo-cortical pathway because they are completely abolished when collicular lesions are added to the V1 lesions (Rodman et al., 1990). Thus we may infer that MT receives some motion information from sources other than V1 (most likely the pulvinar; Bender, 1982), or that MT itself is able to extract some local motion information in the absence of directional inputs.

Consistent with previous analyses of direction selectivity in V1 (Movshon et al., 1985; Emerson et al., 1992), the cells that project to MT may be regarded as local motion energy filters (Adelson

and Bergen, 1985; Heeger, 1987; Grzywacz and Yuille, 1990). Such neurons respond to the motion of image constituents within particular bandpass limits for orientation and spatial and temporal frequency. Each individual neuron, therefore, can only signal motion orthogonal to its preferred orientation. A complex visual stimulus typically contains many oriented components, and the true motion of the stimulus can only be computed by appropriately combining local motion measurements of the sort provided by V1 neurons. Pattern direction-selective neurons, which reflect this higher-order computation of global motion, comprise roughly one-third of the neurons in MT (Movshon et al., 1985; Rodman and Albright, 1989) and may exist in small numbers in V2 (Levitt et al., 1994). Thus our results confirm the suggestion that the computation of pattern motion is at least a two-stage process (Adelson and Movshon, 1982). The transformation from component to pattern motion sensitivity is accomplished by neural circuitry *following* V1 in the central visual pathway and, for the most part, following V2 as well. The most likely loci for this computation appear to be MT itself and V3, an extrastriate area that receives a substantial input from layer 4b of V1 (Felleman et al., 1996), sends ascending projections to MT (Maunsell and Van Essen, 1983; Ungerleider and Desimone, 1986; Shipp and Zeki, 1989), and contains numerous direction-selective neurons (Felleman and Van Essen, 1987). An assessment of component and pattern direction selectivity in V3 suggests that sensitivity to pattern motion is also present in a substantial minority of neurons there (Gegenfurtner et al., 1994), implying that the computation may proceed in several stages or in parallel in V3 and MT.

Finally, our results provide confirmation that the morphological specificity with which different cell types in V1 make their output projections to other areas (e.g., Lund, 1988) is matched by a comparable physiological specificity. It is thus reasonable to think of V1 as a vast "clearing house" that dispatches specific preliminary analyses of the visual scene to the various extrastriate areas responsible for elaborating those analyses into perception and action.

REFERENCES

Adelson EH, Bergen JR (1985) Spatio-temporal energy models for the perception of motion. J Opt Soc Am [A] 2:284–299.

Adelson EH, Movshon JA (1982) Phenomenal coherence of moving visual patterns. Nature 300:523–525.

Allman JM, Kaas JH (1971) A representation of the visual field in the caudal third of the middle temporal gyrus of the owl monkey (*Aotus trivirgatus*). Brain Res 31:85–105.

Bender DB (1982) Receptive-field properties of neurons in the macaque inferior pulvinar. J Neurophysiol 48:1–17.

Bishop PO, Burke W, Davis R (1962) Single-unit recording from antidromically activated optic radiation neurones. J Physiol (Lond) 162:432–450.

Blasdel GG, Lund JS, Fitzpatrick D (1985) Intrinsic connections of macaque striate cortex: axonal projections of cells outside lamina 4c. J Neurosci 5:3350–3369.

Blasdel GG, Fitzpatrick D (1984) Physiological organization of layer 4 in macaque striate cortex. J Neurosci 4:880–895.

Derrington AM, Lennie P (1984) Spatial and temporal contrast sensitivities of neurones in lateral geniculate nucleus of macaque. J Physiol (Lond) 357:219–240.

DeValois RL, Albrecht DG, Thorell LG (1982) Spatial frequency selectivity of cells in macaque visual cortex. Vision Res 22:545–559.

Dow BM (1974) Functional classes of cells and their laminar distribution in monkey visual cortex. J Neurophysiol 37:927–946.

Emerson RC, Bergen JR, Adelson EH (1992) Directionally selective complex cells and the computation of motion energy in cat visual cortex. Vision Res 32:203–218.

Felleman DJ, Van Essen DC (1987) Receptive field properties of neurons in area V3 of macaque monkey extrastriate cortex. J Neurophysiol 57:889–920.

Felleman DJ, Burkhalter A, Van Essen DC (1996) Cortical connections of areas V3 and VP of macaque monkey extrastriate visual cortex. J Comp Neurol, in press.

Ferrera VP, Wilson HR (1990) Perceived direction of moving two-dimensional patterns. Vision Res 30:273–287.

Gallyas F (1979) Silver staining of myelin by means of physical development. Neurol Res 1:203–209.

Gegenfurtner KR, Kiper DC, Levitt JB (1994) Analysis of color and motion in macaque area V3. Soc Neurosci Abstr 20:1741.

Gilbert CD (1977) Laminar differences in receptive field properties of cells in cat primary visual cortex. J Physiol (Lond) 268:391–421.

Girard P, Salin PA, Bullier J (1992) Response selectivity of neurons in area MT of the macaque monkey during reversible inactivation of area V1. J Neurophysiol 67:1437–1446.

Gizzi MS, Katz E, Schumer RA, Movshon JA (1990) Selectivity for orientation and direction of motion of single neurons in cat striate and extrastriate visual cortex. J Neurophysiol 63:1529–1543.

Grzywacz NM, Yuille AL (1990) A model for the estimate of local image velocity by cells in the visual cortex. Proc R Soc Lond [Biol] 239:129–161.

Hawken MJ, Parker AJ, Lund JS (1988) Laminar organization and contrast sensitivity of direction-selective cells in the striate cortex of the old world monkey. J Neurosci 8:3541–3548.

Hawken MJ, Shapley RM, Grosof DH (1996) Temporal frequency selectivity in monkey visual cortex. Vis Neurosci 13:477–492.

Heeger DJ (1987) Model for the extraction of image flow. J Opt Soc Am [A] 4:1455–1471.

Hubel DH, Wiesel TN (1968) Receptive fields and functional architecture of monkey striate cortex. J Physiol (Lond) 195:215–243.

Levitt JB, Kiper DC, Movshon JA (1994) Receptive fields and functional architecture of macaque V2. J Neurophysiol 71:2517–2542.

Livingstone MS, Hubel DH (1984) Anatomy and physiology of a color system in the primate visual cortex. J Neurosci 4:309–356.

Lund JS (1988) Anatomical organization of macaque monkey striate visual cortex. Annu Rev Neurosci 11:253–288.

Lund JS, Lund RD, Hendrickson AE, Bunt AH, Fuchs AF (1976) The origin of efferent pathways from the primary visual cortex, area 17, of the macaque monkey as shown by retrograde transport of horseradish peroxidase. J Comp Neurol 164:287–304.

Maunsell JHR, Van Essen DC (1983) The connections of the middle temporal visual area (MT) and their relationship to a cortical hierarchy in the macaque monkey. J Neurosci 3:2563–2586.

Maunsell JHR, Nealey TA, DePriest DD (1990) Magnocellular and parvocellular contributions to responses in the middle temporal visual area (MT) of the macaque monkey. J Neurosci 10:3323–3334.

Merrill EG, Ainsworth A (1972) Glass-coated platinum-plated tungsten microelectrode. Med Biol Eng 10:495–504.

Movshon JA, Newsome WT (1984) Functional characteristics of striate cortical neurons projecting to MT in the macaque. Soc Neurosci Abstr 10:933.

Movshon JA, Thompson ID, Tolhurst DJ (1978) Spatial summation in the receptive fields of simple cells in the cat's striate cortex. J Physiol (Lond) 283:79–99.

Movshon JA, Adelson EH, Gizzi MS, Newsome WT (1985) The analysis of moving visual patterns. In: Pattern recognition mechanisms (Chagas C, Gattass R, Gross C, eds), pp 117–151. New York: Springer.

Palmer LA, Rosenquist AC (1974) Visual receptive fields of single striate cortical units projecting to the superior colliculus in the cat. Brain Res 67:27–42.

Rodman HR, Albright TD (1989) Single-unit analysis of pattern-motion selective properties in the middle temporal visual area (MT). Exp Brain Res 75:53–64.

Rodman HR, Gross CG, Albright TD (1989) Afferent basis of visual response properties in area MT of the macaque. I. Effects of striate cortex removal. J Neurosci 9:2033–2050.

Rodman HR, Gross CG, Albright TD (1990) Afferent basis of visual response properties in area MT of the macaque. II. Effects of superior colliculus removal. J Neurosci 10:1154–1164.

Shipp S, Zeki S (1989) The organization of connections between areas V5 and V1 in macaque monkey visual cortex. Eur J Neurosci 1:309–332.

Skottun BC, DeValois RL, Grosof DH, Movshon JA, Albrecht DG, Bonds AB (1991) Classifying simple and complex cells on the basis of response modulation. Vision Res 31:1079–1086.

Spatz WB (1977) Topographically organized reciprocal connections between areas 17 and MT in the marmoset *Callithrix jacchus*. Exp Brain Res 27:559–572.

Stoner GR, Albright TD (1994) Visual motion integration: a neurophysiological and psychophysical perspective. In: Visual detection of motion (Smith AT, Snowden RJ, eds). London: Academic.

Tigges J, Tigges M, Anschel S, Cross NA, Letbetter WD, McBride RL (1981) Areal and laminar distribution of neurons interconnecting the central visual cortical areas 17, 18, 19 and MT in the squirrel monkey (*Saimiri*). J Comp Neurol 202:539–560.

Ungerleider LG, Desimone R (1986) Cortical connections of visual area MT in the macaque. J Comp Neurol 248:190–222.

Ungerleider LG, Mishkin M (1979) The striate projection in the superior temporal sulcus of *Macaca mulatta*: location and topographic organization. J Comp Neurol 188:347–366.

Van Essen DC, Maunsell JHR, Bixby JL (1981) The middle temporal visual area in the macaque: myeloarchitecture, connections, functional properties and topographic representation. J Comp Neurol 199:293–326.

Van Essen DC, Newsome WT, Maunsell JHR (1984) The visual field representation in striate cortex of the macaque monkey: asymmetries, anisotropies, and individual variability. Vision Res 5:429–448.

Weller RE, Wall JT, Kaas JH (1984) Cortical connections of the middle temporal visual area (MT) and the superior temporal cortex (ST) in owl monkeys. J Comp Neurol 228:81–104.

Wilson H, Ferrera V, Yo C (1992) A psychophysically motivated model for two-dimensional motion perception. Vis Neurosci 9:79–97.